INTERNATIONAL JOURNAL FOR NUMERICAL METHODS IN FLUIDS, VOL. 20, 803–817 (1995)

TURBULENCE MODELS FOR UNSTRUCTURED FINITE ELEMENT CALCULATIONS

DAVID L. MARCUM*

MSU/NSF Engineering Research Center and Department of Mechanical Engineering, Mississippi State University, U.S.A.

NIGEL P. WEATHERILL†

Department of Civil Engineering, University College of Swansea, SA2 8PP, U.K.

SUMMARY

An unstructured finite element method is presented for calculation of turbulent flow fields about aerospace configurations. Algebraic, one-equation, and two-equation turbulence models are implemented and compared. A new procedure for implementing an unstructured algebraic model without an auxiliary structured grid is presented. The overall procedure is applied to simulation of flow about launch vehicle configurations. The turbulence models are evaluated for calculation of flow fields about a forebody with shock induced separation. For this case, the one-equation model gives better predictions. An inviscid flow field about a complete launch vehicle with multiple boosters is also evaluated to demonstrate the overall procedure.

KEY WORDS: unstructured grids; finite element; turbulence

INTRODUCTION

Solution-adaptive unstructured grid technology is a promising approach offering geometric flexibility for the handling of both complex geometry and flow fields. As such, it can provide a capability to accurately compute complex flow fields about aerospace configurations. Several procedures for calculating inviscid flow fields have been developed and successfully applied to complex configurations. For calculating three-dimensional viscous flow fields, considerably less work has been published using unstructured grids, examples of which are presented in References 1–4. Based on the successful inviscid flow results and the promising but limited results for viscous flow, there is a need for considerably more research into applying unstructured technology to viscous flow fields.

The long-term objective of this work is to develop a computational procedure to predict viscous flow fields about aerospace configurations using unstructured grid technology. For the present work, the objectives are to implement and evaluate various turbulence models and apply the current procedure to simulation of flow about launch vehicle configurations.

* Associate Professor, Mechanical Engineering, Member AIAA
† Reader and Visiting Professor, NSF Engineering Research Center, Mississippi State University, Member AIAA

CCC 0271–2091/95/080803–15

GOVERNING EQUATIONS

The Reynolds-averaged Navier–Stokes equations for time-dependent, three-dimensional, compressible flow of a simple system in thermodynamic equilibrium in the absence of body forces can be expressed in conservation form as

$$\frac{\partial U}{\partial t} + \frac{\partial F^i}{\partial x^i} - \frac{\partial G^i}{\partial x^i} = 0, \quad i = 1, 2, 3 \tag{1}$$

where U is the solution vector, F^i is the advective flux vector in the i-direction, and G^i is the diffusive flux vector in the i-direction. The solution, inviscid flux, and viscous flux vectors are given by

$$U = \begin{bmatrix} \rho \\ \rho V^1 \\ \rho V^2 \\ \rho V^3 \\ \rho E \end{bmatrix}, \quad F^i = \begin{bmatrix} \rho V^1 \\ \rho V^1 V^i + \delta^{1,i} P \\ \rho V^2 V^i + \delta^{2,i} P \\ \rho V^2 V^i + \delta^{3,i} P \\ (\rho E + P) V^i \end{bmatrix}, \quad G^i = \begin{bmatrix} 0 \\ \tau^{1i} \\ \tau^{2i} \\ \tau^{3i} \\ q^i + V^k \tau^{ki} \end{bmatrix}$$

where ρ is the density, V^i is the velocity component in the i-direction, E is the total energy, P is the static pressure, q^i is the heat flux component in the i-direction, τ^{ij} is the viscous stress i, j component. The heat flux and viscous stress components are given by

$$q^i = k_e \frac{\partial T}{\partial x^i}, \qquad \tau^{ij} = \mu_e \left(\frac{\partial V^i}{\partial x^j} + \frac{\partial V^j}{\partial x^i} \right) - \frac{2}{3} \mu_e \delta^{i,j} \frac{\partial V^k}{\partial x^k} \tag{2}$$

where T is the temperature, k_e is the effective coefficient of thermal conductivity, and μ_e is the effective coefficient of viscosity. The effective coefficients are obtained from the sum of the molecular and turbulent coefficients. For the molecular coefficient of viscosity, Sutherland's formula is used. The turbulent coefficient of viscosity is obtained from one of the turbulence models described in the next section. For the coefficients of thermal conductivity, the Prandtl numbers are used.

In the present work a thermally and calorically perfect gas is assumed and the equations of state for pressure and temperature are obtained from perfect gas relationships. Other thermodynamic models for real gas effects, including chemical reactions, have been incorporated. The long-term scope of the present effort includes simulation of plumes, which may require use of these models.

TURBULENCE MODELS

For flow fields about many aerospace configurations, an inviscid or laminar flow assumption is not valid. Consequently, a turbulence model must be incorporated to account for the effects of turbulence. For configurations with limited flow separation, an algebraic Baldwin–Lomax model has been implemented. With flow separation and/or complicated detached viscous regions, a field equation model is more appropriate. The one-equation Baldwin–Barth and two-equation (k–ε) Launder–Sharma models have both been implemented.

Algebraic model

An unstructured version of the algebraic turbulence model of Baldwin and Lomax[5] has been implemented. Rostrand[6] and Mavriplis[7] have incorporated this model into unstructured flow solvers using an auxiliary structured grid. In this approach, the flow properties are interpolated from the unstructured grid to the locally structured grid. The turbulent coefficient of viscosity is determined from the algebraic model using the structured grid data and then interpolated back to the unstructured grid. Pan and Cheng[8] have also incorporated the algebraic model of Baldwin and Barth in a two-dimensional unstructured flow solver. In their approach, an auxiliary grid is used only to sort the unstructured grid into strips for determining the local length scales. No interpolation is required between grids. For the current implementation, a new approach has been used, wherein existing nodes in the unstructured grid are linked together to form a network of lines emanating from solid boundaries. With this approach, no interpolation between grids is required, only the connectivity of the auxiliary grid is needed, and the auxiliary grid is a subset of the full grid. Unstructured algebraic turbulence model grid lines for a regular and irregular unstructured grid are illustrated in Figure 1. This approach is most amenable to unstructured grids which are generally regular as should be the case within the boundary layer region of a quality unstructured grid. It is reasonable to anticipate that even for complex configurations or solution-adapted grids an unstructured grid can be generated in the viscous region which is at least locally regular. The irregularity of the grid lines can be minimized to some extent by setting the local length scales to the distance from the boundary in a direction normal to the surface rather than the distance along the edge. Even with a fully irregular grid, the results are comparable to those for a regular grid. In comparison to an auxiliary grid scheme, the present approach can be viewed as similar, with no interpolation in the direction normal to the boundary and zeroth-order interpolation in the tangential direction. The interpolation error is compatible with the flow field as the gradients normal are typically much greater than those tangential. Although not yet implemented, the procedure described here can be extended for wakes. In the wake, a suitable starting location and normal direction would be required to generate turbulence grid lines. Given corresponding grid lines for a wake point, the procedure presented by Mavriplis[7] could be used to determine the wake centreline and appropriate length scales.

Two-equation turbulence model

For flow fields with significant separation and/or detached viscous regions, a field equation model is more appropriate than the previously described algebraic model. A two-equation k–ε

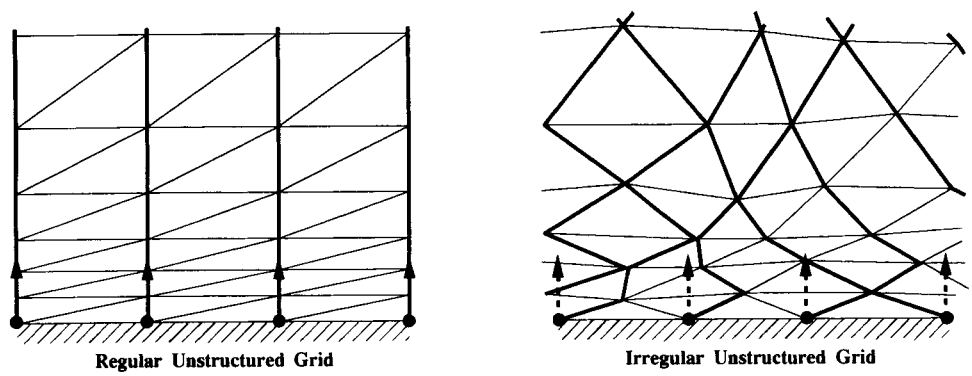

Figure 1. Unstructured algebraic turbulence model grid lines

turbulence model[9-11] has been implemented. The model used in the low Reynolds number model of Launder and Sharma.[11] With a k–ε model the turbulent coefficient of viscosity is determined from the turbulence kinetic energy and dissipation rate which are obtained from coupled transport equations. These equations are solved in the same manner as the Navier–Stokes equations in the present implementation.

Typically, a y^+ value near 1 is required for reasonable accuracy. The resulting stiffness can affect the robustness and efficiency of the flow solver. In addition, initial conditions, boundary conditions, limiters, and dissipation can significantly impact robustness. The following conditions drastically improve the performance with the present flow solver:

(a) Set k and ε initially to values that correspond to high levels of turbulence, e.g. a turbulence intensity of 10 per cent and a turbulence Reynolds number of 500. This typically ensures that turbulence is produced.
(b) Set k and ε boundary conditions to physically realistic values that correspond to low levels of turbulence, e.g. a turbulence intensity of 1 per cent and a turbulence Reynolds number of 0·1. This typically produces solutions that are independent of the far-field turbulence.
(c) Limit k and ε so that they do not go negative in value during initial transients.
(d) Limit the maximum turbulent viscosity during initial transients and if there is poor grid resolution in high gradient regions. Typically, a maximum ratio of turbulent to molecular viscosity of 10 000 is used. In severe cases (poor grid resolution and separation) a lower maximum may be required, e.g. 500–1000.
(e) Add artificial dissipation predominantly in the direction of velocity (a first-order upwind solver can produce the equivalent). The flow field solution was found to be relatively insensitive to reasonable levels of streamwise dissipation added to the k–ε equations. However, the robustness of the flow solver increased with added k–ε dissipation. This additional dissipation is not added to the Navier–Stokes equations.

One-equation turbulence model

For flow fields with significant separation, the previously described models have in general been successful only in a limited number of cases. The one-equation model developed by Baldwin and Barth[12] has produced significantly improved results for transonic flow fields about aerofoil configurations with shock induced separation. This model has been implemented in the present procedure as an alternative to the two-equation model. With the one-equation model, the turbulent coefficient of viscosity is determined from a modified turbulence Reynolds number which is obtained from a single transport equation. This equation is solved in the same manner as the Navier–Stokes equations in the present implementation.

Typically, a y^+ value near 2 is required for reasonable accuracy, which is an improvement over the k–ε model. Also, in comparison with the k–ε model, the one-equation model is more robust and less sensitive to initial conditions, boundary conditions and limiters with the present flow solver. As was the case for the k–ε model, the solution was found to be relatively insensitive to reasonable levels of streamwise dissipation. However, for this model, streamwise dissipation was found to be essential for non-oscillatory solutions. Again, this additional dissipation is not added to the Navier–Stokes equations.

In the present implementation, the anti-diffusive term is not limited for positivity, as was done in the original implementation.[12] Streamwise dissipation was found to be sufficient for relatively coarse grids (yet fine enough for reasonable accuracy) where the turbulent coefficient of viscosity at adjacent nodes varied in some regions by a factor of three or more. Limiting alone was also

found to be sufficient for smooth solutions. However, even partial limiting significantly degraded the solution and increased the resulting skin friction. Streamwise dissipation did not degrade the solution.

SOLUTION PROCEDURE

The governing equations are discretized in space using a Galerkin weighted residual approximation with the solution domain divided into tetrahedral finite elements. The discretization is vertex based and the solution vector is stored and solved for at the element vertices or nodes. Time discretization is obtained using either an explicit multistep Runge–Kutta scheme or an explicit two-step Lax–Wendroff scheme. The Runge–Kutta scheme is based on the procedures developed in References 2, 13 and 14, and the Lax–Wendroff scheme is based on the procedures developed in References 2, 15 and 16. For the present work, only the Lax–Wendroff scheme has been used. Boundary conditions are implemented using a method of characteristics procedure described in Reference 2.

Finite element discretization

For the governing equations, the Galerkin weighted residual statement is given by

$$\int \psi \left[\frac{\partial \hat{U}}{\partial t} + \frac{\partial \hat{F}^i}{\partial x^i} - \frac{\partial \hat{G}^i}{\partial x^i} \right] \mathrm{d}\Omega = 0 \tag{3}$$

where ψ is the test function, Ω is the domain and $\hat{}$ denotes approximated values obtained using a finite element shape function, ϕ. At each node in the domain, the weighted residual statement can be integrated directly using a piecewise linear test function. For the time derivative, a piecewise linear shape function is used and the resultant mass matrix is lumped for steady flow calculations. A piecewise linear shape function is used to evaluate the viscous flux vector at time level n. The inviscid flux vector is evaluated at time level $n + \frac{1}{2}$ with a piecewise constant shape function. The integrated result for equation (3), using the Gauss divergence theorem, can be expressed for node k as

$$\sum_{je} \sum_{j} M_{je_{j,k}} \left(\frac{U^{n+1} - U^n}{\Delta t} \right)_{je_j} - \sum_{je} \frac{\partial \phi}{\partial x^i} je_k (F_{je}^{i\,n+1/2} - G_{je}^{i n}) \Omega_{je}$$

$$- \sum_{jeb} \frac{\partial \phi}{\partial x^i} jeb_{nb} (F_{jeb}^{i\,n+1/2} - G_{je}^{i n}) \Omega_{jeb} = 0 \tag{4}$$

where j denotes an element node, je denotes an element, jeb denotes a boundary element, nb denotes the element node opposite a boundary face, Ω denotes the element volume, M is the mass matrix, and Δt is the time step. The boundary term in equation (4) contributes only if node k is on a boundary. The linear shape function partial derivative is given by

$$\frac{\partial \phi}{\partial x^i} je_j = -\frac{1}{3} \left(\frac{\Gamma_{je}^i}{\Omega_{je}} \right) \tag{5}$$

where Γ_{je}^i is the area component in the i-direction for the element surface opposite node j of element je. The solution vector for the inviscid flux vector at time level $n + \frac{1}{2}$ is obtained by integrating equation (3) without the viscous term and with a piecewise constant test function and

linear shape function. The result is

$$U_{je}^{n+1/2} = \frac{1}{4}\sum_j U_{je_j}^n - \frac{1}{2}\Delta t_{je}\sum_j \frac{\partial \phi}{\partial x_i} je_j F_{je_j}^{in} \tag{6}$$

where Δt_{je} is the element time step. The viscous flux vector is evaluated directly from the solution vector at the nodes. For example, the heat flux component is given by

$$G_{je}^i = \frac{1}{4}\left(\sum_j k_{e_{je_j}}\right)\sum_j \frac{\partial \phi}{\partial x^i} je_j T_{je_j}\Omega_{je} \tag{7}$$

The other components of the viscous flux vector are obtained in a similar manner. The time step in equations (4) and (6) is set to the local maximum permissible time step for steady flow calculations.

Local structured edge connectivity

Many finite element and finite volume flow solvers can be implemented using either an edge, element or face based data structure. For example, the equivalent of equation (4) for the Runge–Kutta solver can be expressed in edge based form. The edge based data structure can offer memory and speed advantages. It can also be used to exploit local structure in the grid. An edge based data structure that utilizes a local structured edge connectivity has been developed.[17] Neighbouring edges and their connectivity for this data structure are shown in Figure 2 for a two-dimensional unstructured grid. For an edge given by points 1 and 2, two closely aligned neighbouring edges given by points 0 and 1 and points 2 and 3 are selected. Points 0, 1, 2 and 3 are analogous to locations $i-1$, i, $i+1$ and $i+2$ in a structured grid. Ideally, the connected edges should form a very smooth line. For a typical grid, however, with varying element volumes, there will be some connected edges which do not form a smooth line. Based on results obtained with such connections, this does not create any numerical problems. The local structured edge connectivity allows direct and efficient implementation of many upwind high-resolution structured schemes. In the present work, a structured flux-limited dissipation model is implemented using this connectivity.

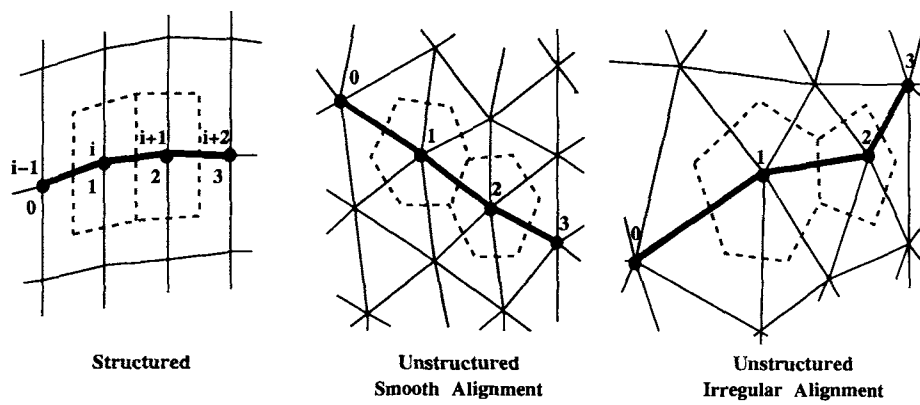

Figure 2. Local structured edge connectivity

Artificial dissipation

In regions containing severe gradients, e.g. near shock waves and stagnation points, artificial dissipation is required to filter out oscillations. Also, appropriately scaled background dissipation for the turbulence unknowns is beneficial with the field equation turbulence models previously described. For the Lax–Wendroff solver used in the present work, an adaptive second-order dissipation model is used. The second-order dissipation model is given by

$$D_k = \sum_{\text{edge}} \max(c_1, c_2 G)\, S(U_2 - U_1) \tag{8}$$

where D_k is the dissipation term for node k which is added to the right-hand side of equation (4), U_1 and U_2 are the solution vectors at locations 1 and 2 in Figure 2, c_1 is the background constant, c_2 is the gradient switch constant, G is the gradient switch and S is the directional scaling factor. Typically, the background constant is set to zero, turning off the background dissipation. However, for the turbulence transport equations a value of 0·5 is typically used. This provides levels of dissipation near or above that of a first-order upwind scheme. The gradient switch is given by

$$G = \max\left[\left|\frac{p_0 + p_2 - 2p_1}{p_0 + p_2 + 2p_1}\right|, \left|\frac{p_1 + p_3 - 2p_2}{p_1 + p_3 + 2p_3}\right|\right] \tag{9}$$

where p is typically the pressure. The gradient switch is also normalized so that it varies between 0 and 1. The directional scaling factor is obtained using edge average variables and is given by

$$S = V^i \cdot \Gamma^i + a|\Gamma^i| \tag{10}$$

where a is the speed of sound, V^i is the velocity vector, and Γ^i is the edge area vector. The scaling factor can be modified to provide dissipation primarily in the direction of velocity as given by

$$\tilde{S} = \frac{V^i \cdot \Gamma^i}{|V^i|\,|\Gamma^i|} S \tag{11}$$

The modified scaling factor is always used for the turbulence transport equations.

For high Mach number flow fields, a limiting modification provides improved resolution. This model is an unstructured implementation of the flux-limited model developed by Jameson[18] and enhanced by Yoon and Kwak.[19] Using the local structured edge connectivity, this model can be obtained by modifying the gradient switch constant as given by

$$\tilde{c}_2 = c_2\left\{2 - \max\left[\min\left(\frac{U_1 - U_0}{U_2 - U_1}, 1\right), 0\right] - \max\left[\min\left(\frac{U_3 - U_2}{U_2 - U_1}, 1\right), 0\right]\right\} \tag{12}$$

Computer implementation

The numerical procedures described above have been implemented in a computer code which has been installed and executed on a wide variety of computers. On vector computers the code is completely vectorized with the exception of some setup and output routines. Memory requirements vary between 100 and 200 words per node depending on options selected and maximum vector length used for work arrays and colouring. On the CRAY C90 at NASA Ames Research Center the code requires 9, 18, 24 and 28×10^{-6} CPU seconds per iteration per point for inviscid, viscous with algebraic model, viscous with one-equation model, and viscous with two-equation model respectively. The memory and CPU requirements given are for three-dimensional cases.

GRID GENERATION

The three dimensional unstructured tetrahedral grids used in the present work were obtained from a Delaunay based grid generator developed by Weatherill.[17,20] This generator uses the Delaunay triangulation criterion with automatic point insertion. A grid of 1 million elements can be generated in 10–30 min on commonly used workstations.[17] These times are for the complete generation process, from surface definition to final grid in a form such that it can be used directly by the flow solver.

At present our grid generation capability for viscous flow fields is limited. A semi-structured approach has been taken wherein the surface grid is displaced and a semi-structured boundary layer grid is inserted. The boundary-layer grid is generated by stacking the unstructured surface grid to form the field grid. The initial capability was developed by Halt.[21] While this approach has limited geometric flexibility, it is suitable for many launch vehicle configurations and can be used with unstructured solution adaptation. With further development, this approach should provide a capability adequate for most launch vehicles.

RESULTS

The procedures described above have been successfully applied to a wide variety of aerospace applications.[2,17,20] Several flow fields have been computed for this investigation to verify and compare the accuracy of the turbulence models and demonstrate the present capability for launch vehicle configurations.

Turbulent flow over a flat plate

A detailed study has been completed for laminar and turbulent flow over a flat plate to verify the accuracy of the computed results for simple viscous flow fields. Very accurate solutions can be obtained with the unstructured solver using a grid with moderate density. For laminar flow, the Blassius solution can be accurately predicted using the unstructured equivalent of a 21×21 structured grid.[2] The unstructured solver has also been compared directly with a fully structured solver. The results for a regularly connected grid are very similar to those of the structured solver.

For turbulent flow, various grid types, as illustrated in Figure 3, have been evaluated. In general, the accuracy is very similar for each grid type. However, the transformed, irregular grid

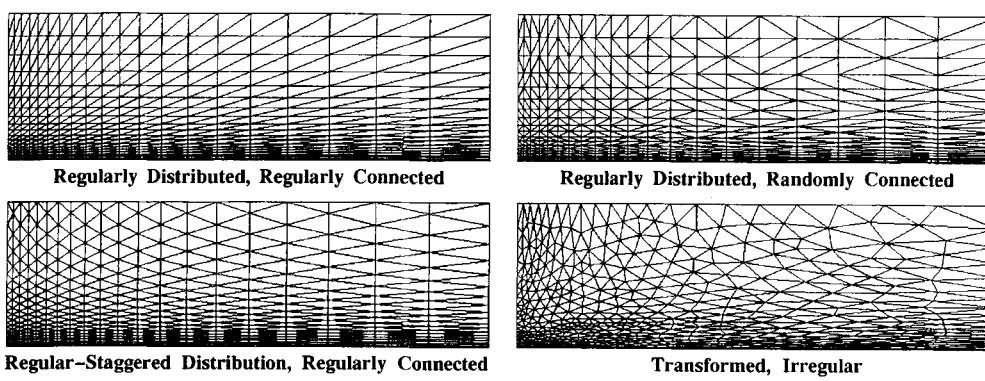

Figure 3. Grids for flat plate flow (y-co-ordinate expanded $10\times$ for clarity)

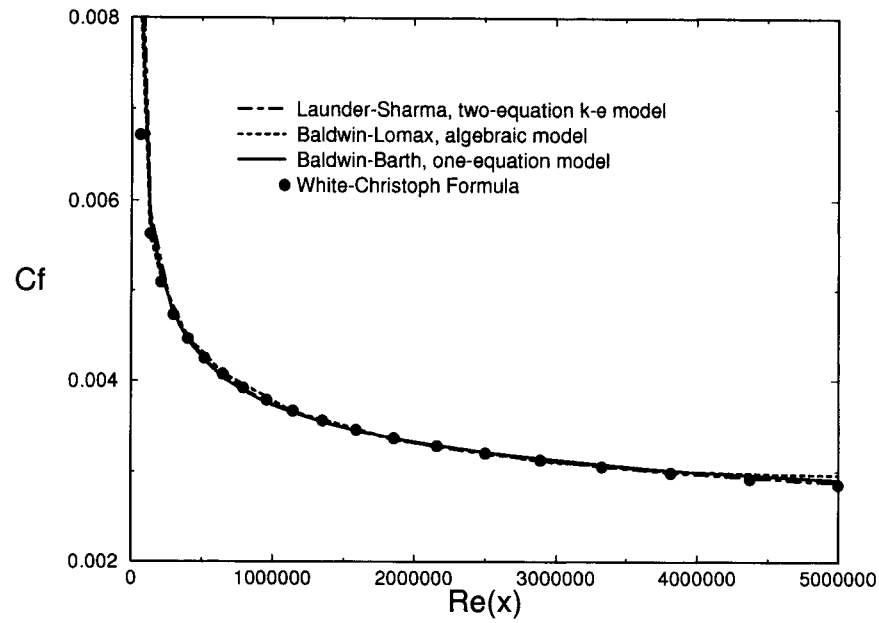

Figure 4. Skin friction distributions for turbulent flat plate flow at $M_\infty = 0{\cdot}5$

did produce local imperfections which diminish as the grid density is increased. With the randomly connected and the staggered grids, the convergence rate was slightly degraded in comparison to the regularly connected grid. The convergence rate for the transformed, irregular grid was significantly degraded.

Distributions of the skin friction coefficient computed with the algebraic, one-equation, and two-equation turbulence models are shown in Figure 4. The results for each model are in excellent agreement with each other and the White–Christoph formula.[22] For the algebraic and one-equation model the nodes adjacent to the flat plate are at a y^+ of ~ 2 and for the two-equation model they are at a y^+ of ~ 1. A regularly connected grid with 441 nodes (equivalent to a 21×21 structured grid) was used for each model. Finer grids and lower y^+ values were also evaluated and no significant differences in the results were found. Higher y^+ values degraded the accuracy of the solutions.

Boundary layer profiles for the three turbulence models at the midpoint of the plate are shown in Figure 5. Again, all three models are in excellent agreement. However, the two-equation model required finer resolution to obtain the same profile as the other models.

Boundary layer profiles, for the algebraic turbulence model, which is grid type dependent in the present implementation, are shown in Figure 6. The profile for the irregular, transformed grid is in good agreement with the profile for the regularly distributed and connected grid. The irregular, transformed grid represents a worst-case scenario for the grid type dependency of the present algebraic model implementation.

Launch vehicle forebody

A launch vehicle forebody was also studied to compare the computed results with experimental data for a flow field with shock induced separation. The geometry is a simple spherically capped,

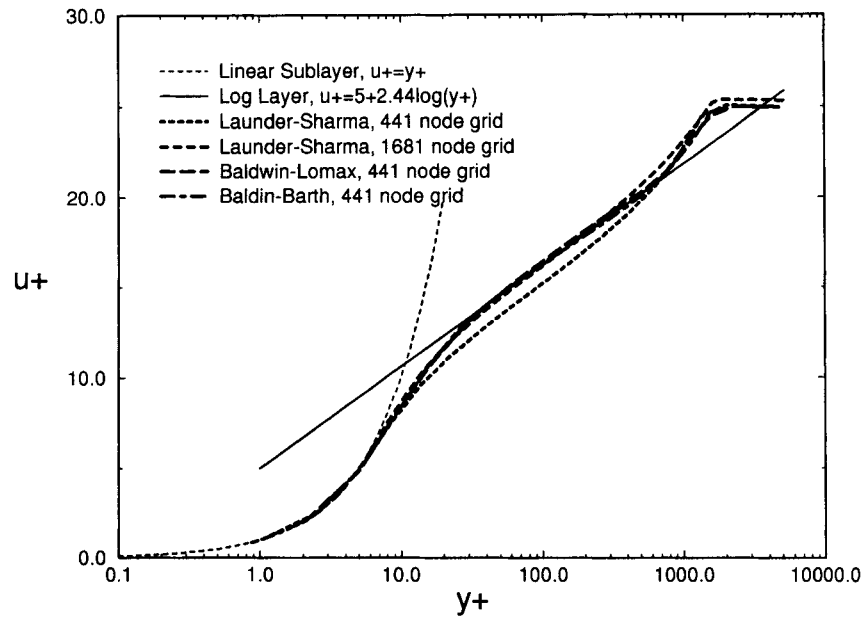

Figure 5. Boundary layer profiles for turbulent flat plate flow

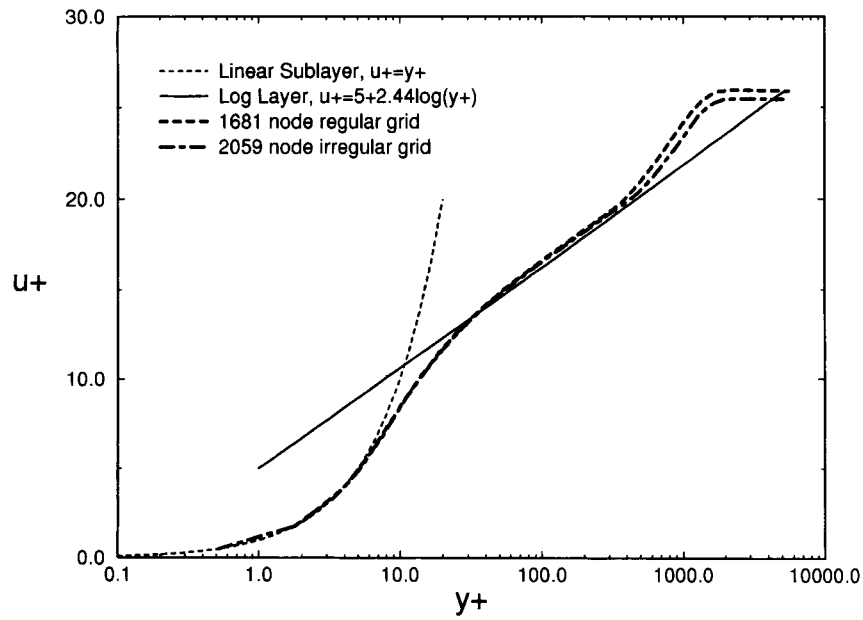

Figure 6. Boundary layer profiles for algebraic turbulence model with different grid types

tangent-cone, cylinder forebody. For a free-stream Mach number of 0·8–0·9, there is a shock induced separation bubble located downstream of the cone–cylinder junction. The surface grid used for this case is illustrated in Figure 7.

Surface pressure coefficient distributions are shown in Figure 8 for experimental data[23] and computed solutions obtained with Euler and Navier–Stokes (with all three turbulence models). As expected the inviscid results compare poorly. The viscous results compare considerably better with the experimental data. Each of the turbulence models predicts separation. While the overall comparison is good, only the one-equation model accurately predicts the extent of the separation bubble. For validation, all of the results were obtained assuming three-dimensional flow.

This case was also computed by Deese *et al.*[24] with an axisymmetric structured solver. Those results were obtained with similar algebraic and k–ε turbulence models. Pressure coefficient distributions for the structured and unstructured solutions are shown in Figure 9. The unstructured results compare slightly better to the experimental data in the shock/separation region and the structured results compare slightly better in the nose region. As the structured results were obtained with a much finer grid (12 000 nodes on the symmetry half-plane versus 2102 nodes), their somewhat better prediction is expected. A finer grid for the unstructured grid should improve the overall prediction. However, based on the structured grid results, it is doubtful that the prediction of the separation region would improve.

This configuration was also evaluated for a fully three-dimensional case at an angle of attack of 4° with the one-equation model. Pressure coefficient distributions are shown in Figure 10. The overall comparison with experimental data is good.

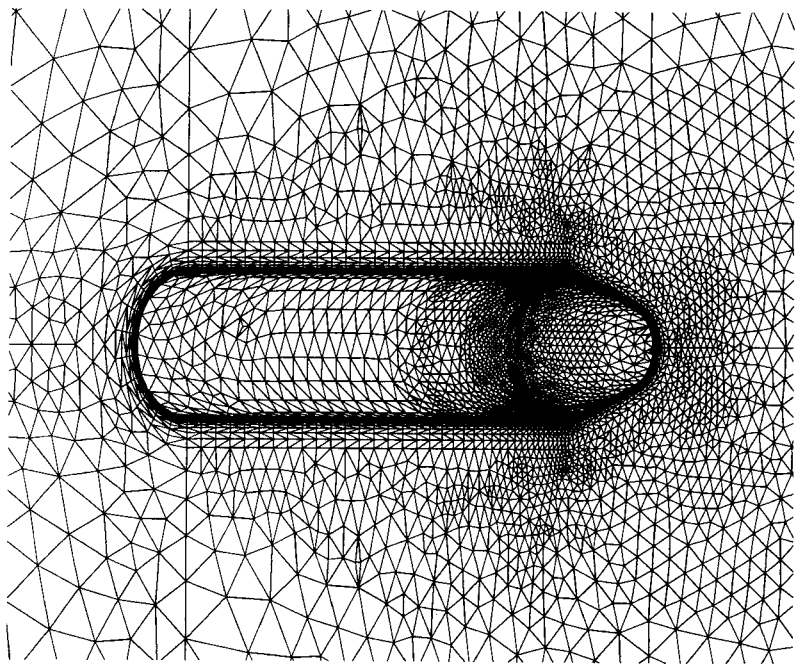

Figure 7. Surface grid for launch vehicle forebody (48 236 nodes and 277 932 elements in complete field grid)

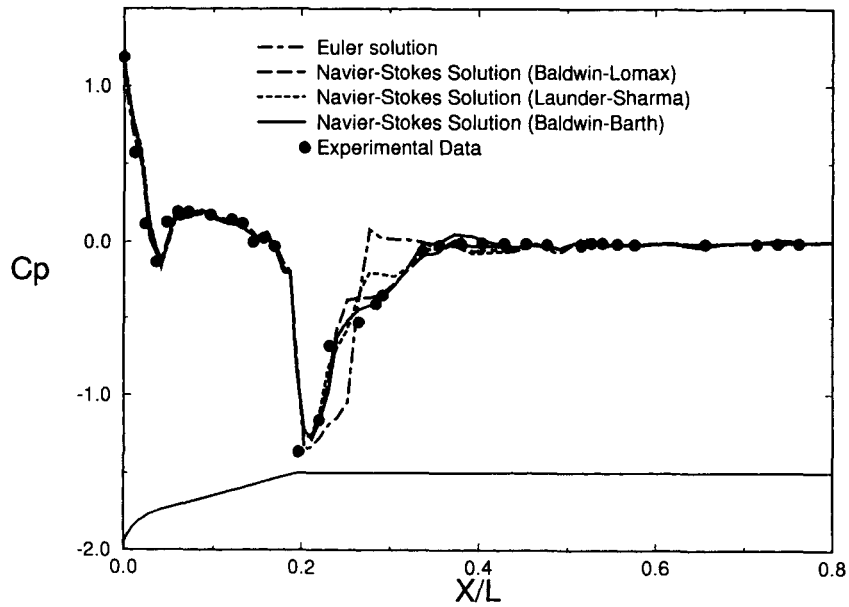

Figure 8. Surface pressure coefficient distributions for launch vehicle at $M_\infty = 0{\cdot}84$, $\alpha = 0°$ and $Re = 4 \times 10^6$/ft

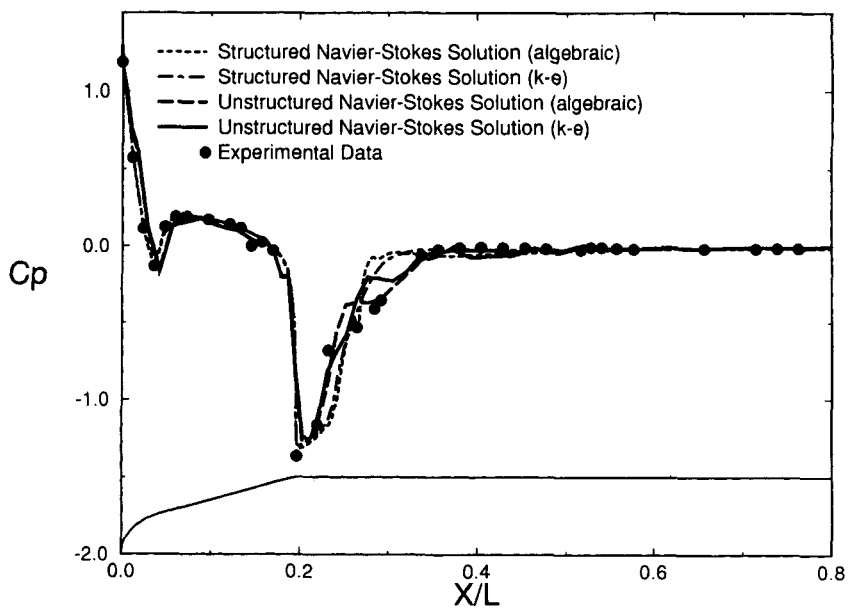

Figure 9. Surface pressure coefficient distributions for structured and unstructured solutions

Launch vehicle with multiple boosters

Inviscid flow about a generic launch vehicle with three additional boosters was computed to demonstrate and evaluate the flow solver for a more realistic configuration. The surface grid for this configuration is illustrated in Figure 11. The National Grid Project (NGP) system[25] was used

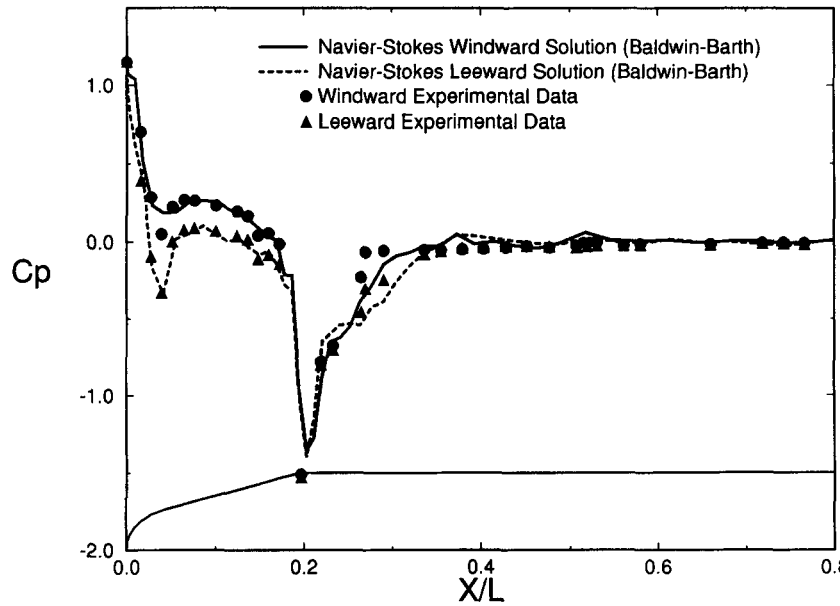

Figure 10. Surface pressure coefficient distributions for launch vehicle at $M_\infty = 0{\cdot}8$, $\alpha = 4^\circ$ and $Re = 4 \times 10^6$/ft

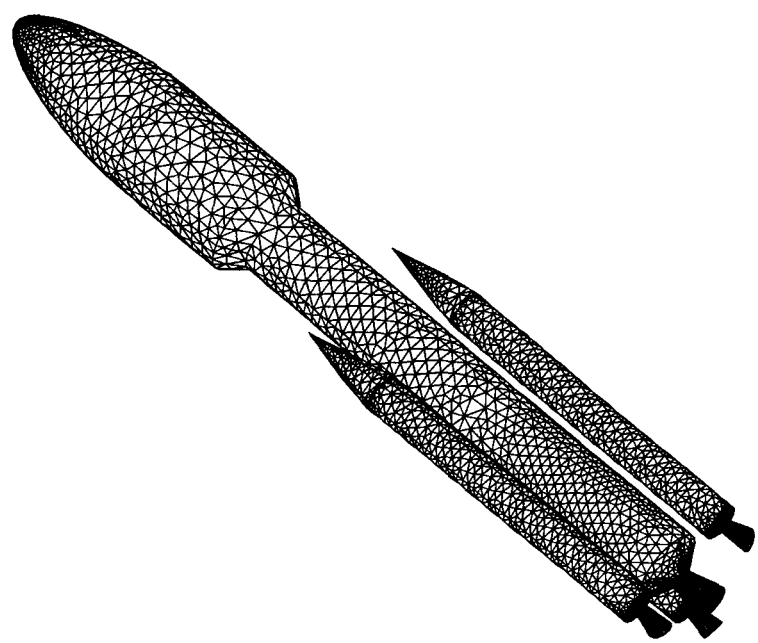

Figure 11. Surface grid for complete launch vehicle (48 993 nodes and 286 059 elements)

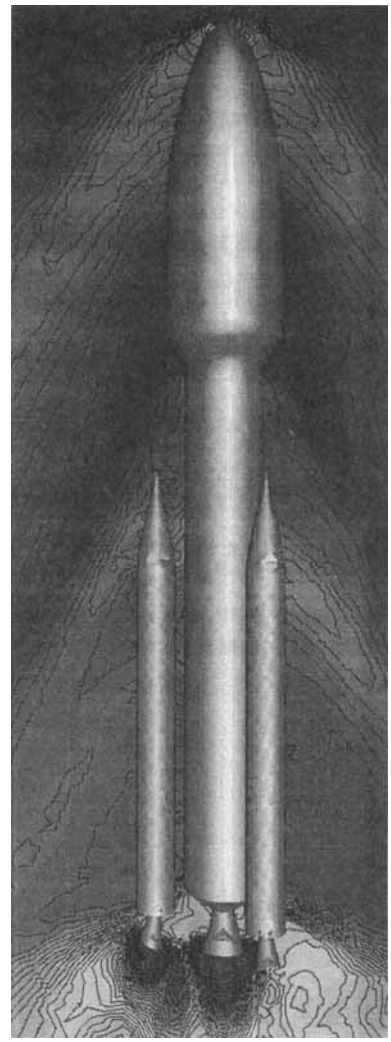

Figure 12. Logarithmic pressure contours for complete launch vehicle at $M_\infty = 2{\cdot}2$ and $\alpha = 0{\cdot}5^\circ$

to define the geometry and generate both the surface and field grid. The rocket motors are each modelled power-on. At the motor exits, the ratio of pressure to far-field pressure is 40–50:1. The area ratio is 10:1 for the main motor and 8:1 for each booster. Logarithmic contours of the pressure are shown in Figure 12. The overall complexity of the flow field is clearly evident. Accurate predictions for this case would require viscous modelling. However, the basic features of the flow field are all present in the inviscid solution.

SUMMARY AND CONCLUSIONS

An unstructured finite element procedure for calculating turbulent flow fields about aerospace configurations has been presented. Algebraic, one-equation, and two-equation turbulence models have been implemented and compared. For flow about a forebody with shock induced separ-

ation, the one-equation model gives better results. Further investigation is required to validate the one-equation model for flow about more complex vehicles. Future work will focus on implementing a more efficient implicit flow solver, further development of semi-structured grid generation methods, and continued investigation of turbulence models.

ACKNOWLEDGEMENTS

The authors would like to thank D. Halt for generating the surface grid for the forebody configuration and J. Whitmire for defining and generating the geometry and surface grid for the multiple booster configuration. Funding for this effort was provided in part from the National Science Foundation, Mississippi State University, and McDonnell Douglas. Computing resources were provided in part by the Numerical Aerodynamic Simulation program at NASA Ames Research Center.

REFERENCES

1. F. Chalot, J. Zdenek, M. Mallet, M. Ravachol and G. Roge, 'Development of finite element Navier–Stokes solver with applications to turbulent and hypersonic flows', *AIAA Paper 92-0670*, 1992.
2. D. Marcum and R. Agarwal, 'A finite element Navier–Stokes solver for unstructured grids', *AIAA j.*, **30**, 648 (1992).
3. O. Hassan, E. B. Probert, K. Morgan and J. Peraire, 'Line relaxation methods for the solution of two-dimensional and three-dimensional compressible flows', *AIAA Paper 93-3366*, 1993.
4. K. Nakahashi, 'Adaptive-prismatic-grid method for external viscous flow computations', *AIAA Paper 93-3314*, 1993.
5. B. Baldwin and H. Lomax, 'Thin layer approximation and algebraic model for separated turbulent flows', *AIAA Paper 78-257*, 1978.
6. P. Rostrand, 'Algebraic turbulence models for the computation of two-dimensional high-speed flows using unstructured grids', *Int. j. numer. methods fluids*, **9**, 1121 (1989).
7. D. J. Mavriplis, 'Algebraic turbulence modeling for unstructured and adaptive meshes', *AIAA j.*, **29**, 2086 (1992).
8. D. Pan and J. Cheng, 'Upwind finite-volume Navier–Stokes computations on unstructured triangular meshes', *AIAA, j.*, **31**, 1618 (1993).
9. W. P. Jones and B. E. Launder, 'The calculation of low-Reynolds-number phenomena with a two-equation model of turbulence', *Int. J. Heat Mass Transfer*, **16**, 1119 (1973).
10. B. E. Launder and D. B. Spalding, 'The numerical computation of turbulent flows', *Comput. Methods Appl. Mech. Eng.*, **3**, 269 (1974).
11. B. Launder and B. Sharma, 'Application of the energy-dissipation model of turbulence to the calculation of flow near a spinning disk', *Lett. Heat Mass Transfer*, **1**, 131 (1974).
12. B. Baldwin and T. Barth, 'A one-equation turbulence transport model for high Reynolds number wall-bounded flows', *NASA TM 102847*, 1990.
13. A. Jameson, T. J. Baker and N. P. Weatherill, 'Calculation of inviscid transonic flow over a complete aircraft', *AIAA Paper 86-0103*, 1986.
14. D. J. Mavriplis, 'Accurate multigrid solution of the euler equations on unstructured and adaptive meshes', *AIAA j.*, **28**, 213 (1990).
15. J. Peraire, J. Peiro, L. Formaggia, K. Morgan and O. C. Zienkiewicz, 'Finite element Euler computations in three dimensions', *AIAA Paper 88-0032*, 1988.
16. R. Löhner, K. Morgan, J. Peraire and M. Vahdati, 'Finite element flux-corrected transport for the Euler and Navier–Stokes equations', *Int. j. numer. methods fluids*, **7**, 1093 (1987).
17. N. Weatherill, O. Hassan and D. Marcum, 'Calculation of steady compressible flowfields with the finite element method', *AIAA Paper 93-0341*, 1993.
18. A. Jameson, 'A non-oscillatory shock capturing scheme using flux limited dissipation', *Lectures Appl. Math.*, **22**, 345 (1985).
19. S. Yoon and D. Kwak, 'Artificial dissipation models for hypersonic external flow', *AIAA Paper 88-3708*, 1988.
20. N. Weatherill, O. Hassan, M. Marchant and D. Marcum, 'Adaptive inviscid flow solutions for aerospace geometries on efficiently generated unstructured tetrahedral meshes', *AIAA Paper 93-3390*, 1993.
21. D. Halt, private communication, 1992.
22. F. M. White and G. H. Christoph, 'A simple theory for the two-dimensional compressible turbulent boundary layer', *J. Basic Eng.*, **94**, 636 (1972).
23. L. Arendt, 'A wind tunnel investigation of the buffet characteristics for the standard 3920 Delta and the Baseline Delta II Medium Launch Vehicles and Mach numbers from 0·6 to 1·5', *AEDC-TSR-87-P15*, 1987.
24. J. Deese, T. Gielda, R. Agarwal and D. Pavish, 'Prediction of flow separation on launch vehicle configurations', *AIAA Paper 91-1727* 1991.
25. J. F. Thompson, 'The National Grid Project', *Comput. Systems Eng.*, **3**, 393 (1992).